Atmospheric Environment 92 (2014) 566–575

Contents lists available at ScienceDirect

Atmospheric Environment

journal homepage: www.elsevier.com/locate/atmosenv

Small-scale spatial variations of gaseous air pollutants – A comparison of path-integrated and *in situ* measurement methods

Hong Ling [a,b], Klaus Schäfer [b], Jinyuan Xin [a], Min Qin [c], Peter Suppan [b], Yuesi Wang [a,*]

[a] State Key Laboratory of Atmospheric Boundary Layer Physics and Atmospheric Chemistry (LAPC), Institute of Atmospheric Physics (IAP), Chinese Academy of Sciences (CAS), Beijing 100029, China
[b] Institute of Meteorology and Climate Research, Department of Atmospheric Environmental Research (IMK-IFU), Karlsruhe Institute of Technology (KIT), Garmisch-Partenkirchen 82467, Germany
[c] Key Laboratory of Environmental Optics and Technology, Anhui Institute of Optics and Fine Mechanics (AIOFM), Chinese Academy of Sciences (CAS), Hefei 230031, China

HIGHLIGHTS

- Differences between path-integrated and *in situ* measurement results were studied.
- Small-scale spatial and temporal variations of 5 pollutants were estimated.
- Meteorological parameters influence the temporal and spatial variations a lot.
- Underlying surface roughness affects spatial variation as well.
- The diurnal variation pattern of HCHO was related to traffic emissions.

ARTICLE INFO

Article history:
Received 10 May 2013
Accepted 27 January 2014
Available online 29 January 2014

Keywords:
DOAS
Traffic-related emissions
Meteorological parameters
Air quality
Urban environment

ABSTRACT

Traffic emissions are a very important factor in Beijing's urban air quality. To investigate small-scale spatial variations in air pollutants, a campaign was carried out from April 2009 through March 2011 in Beijing. DOAS (differential optical absorption spectroscopy) systems and *in situ* instruments were used. Atmospheric NO, NO_2, O_3 and SO_2 mixing ratios were monitored. Meanwhile, HCHO mixing ratios were measured by two different DOAS systems. Diurnal variations of these mixing ratios were analysed. Differences between the path-integrated and *in situ* measurements were investigated based on the results from the campaign. The influences of different weather situations, dilution conditions and light-path locations were investigated as well. The results show that the differences between path-integrated and *in situ* mixing ratios were affected by combinations of emission source strengths, weather conditions, chemical transformations and local convection. Path-integrated measurements satisfy the requirements of traffic emission investigations better than *in situ* measurements.

1. Introduction

Beijing frequently suffers from air pollution. Road traffic is already an important source of air pollution, and it continues to increase (Chan and Yao, 2008; Hao and Wang, 2005; Xin et al., 2010). To determine traffic-related air quality and small-scale spatial variations of air pollutants near a motorway in Beijing, a measurement campaign was carried out. The target compounds were NO, NO_2 and HCHO as primary pollutants and O_3 as a secondary air pollutant. Additionally, SO_2 was of interest for regional air pollution.

NO, NO_2, O_3, SO_2 and HCHO are influenced by chemical and photochemical processes in the lower atmosphere. They are also important for secondary aerosol formation (Seinfeld and Pandis, 1997). NO_x and O_3 are key elements of photochemical reactions in the troposphere, whereas NO_x is an important precursor for ozone chemistry. Furthermore, O_3 is an air pollutant that causes adverse health effects (Ebi and McGregor, 2008). SO_2 is one of the most important sulphur-containing air pollutants. While SO_2 itself is not toxic, its oxidation products can lead to sulphate and acid rain formation. SO_2 is also important for the formation of secondary aerosols (Andreae and Crutzen, 1997; Ravishankara, 1997; Seinfeld and Pandis, 1997). HCHO is one of the most abundant carbonyl compounds in the atmosphere (Ronneau, 1987; Seco et al., 2007). As a photochemically reactive gas, HCHO plays an important role in

* Corresponding author.
E-mail address: wys@mail.iap.ac.cn (Y. Wang).

1352-2310/$ – see front matter © 2014 Elsevier Ltd. All rights reserved.
http://dx.doi.org/10.1016/j.atmosenv.2014.01.062

photochemical reactions, vegetation–atmosphere exchange processes and adverse human health effects (Cavalcante et al., 2006; Grosjean, 1982; Lei et al., 2009).

To better quantify the strong spatial variability of air pollution concentrations near roadways, the research area of this campaign includes a busy motorway. A better understanding of this variability of will aid in determining exposures to and the corresponding health effects from traffic-related air pollution. In this study, traditional methods (*in situ* measurements) for air pollutant measurements could not provide representative results for traffic-related emissions. Thus, a path-integrated method with high temporal resolution and long-term continuous observation was required. This path-integrated method allows measurements to be conducted across a road or motorway.

The DOAS (differential optical absorption spectroscopy) method, which was first introduced by U. Platt and D. Perner (Platt and Perner, 1980; Platt et al., 1979; Platt and Stutz, 2008), was applied. It uses an open light-path instead of traditional sample cells. The length of the light-path can range from 100 m to several km. The overall absorption of a trace gas along the light-path between the light emitter and the receiver is detected, and the DOAS system thus provides an average concentration of a trace gas for the light-path. Due to its high sensitivity, high temporal resolution and fast, continuous measurement of multiple compounds, the open-path technique is now widely used for atmospheric monitoring in both urban and suburban areas (Avino and Manigrasso, 2008; Büns and Kuttler, 2012; Grutter et al., 2003; Schäfer et al., 2005, 2008; Schatzmann et al., 2006; Volz-Thomas et al., 2003). DOAS systems have also been introduced in China and have been implemented in atmospheric environmental monitoring campaigns and research work (Qin et al., 2009; Zhang et al., 2012).

A commercial UV-DOAS system from OPSIS GmbH was used in this campaign. *In situ* instruments were deployed and used for comparison. In this paper, the DOAS measurements of SO_2, NO, NO_2 and O_3 will be compared with the *in situ* measurements. HCHO results will further be compared with the results of another DOAS system built by (AIOFM) (Qin et al., 2006, 2009).

Comparison with *in situ* measurement results will allow the evaluation of DOAS results from the campaign and the investigation of small-scale spatial concentration variations. The representativeness of DOAS results for a traffic emission-influenced area will be studied. The effects of different weather and wind conditions will also be determined.

2. Methodology

2.1. Instruments

The OPSIS UV-DOAS system deployed in this campaign contains an analyser (AR500) and an emitter/receiver unit (ER130) pointing to three retro-reflectors (RR090). The system uses a 150 W xenon short-arc lamp which steadily generates light beams with a spectrum from 200 nm to 700 nm. The receiver unit focuses the reflected light to the end of an optical fibre cable and directs it into the analyser. A fan is installed in the emitter/receiver unit to avoid the influence of O_3 generated by the xenon lamp.

2.2. Instruments used for comparison

A UV photometric O_3 analyser (49i, ThermoFisherScientific, Inc. (TE), USA), a pulsed fluorescence SO_2 analyser (43i, TE) and a chemiluminescence-based NO–NO_2–NO_x analyser (42i, TE) were used for the inorganic gas monitoring comparison. The AIOFM DOAS was used for the evaluation of HCHO monitoring.

2.3. Calibration

The DOAS system requires a regular calibration procedure as the sensitivity of the optical grating in the analyser gradually changes over time. Thus, to determine the reliability of the data, the data were checked against a reference and multi-point calibration of the system. To ensure that the instrument changes do not influence data quality, calibrations are necessary every half year for inorganic gases and every three months for organic gases. An individual calibration system was used for the DOAS calibration, including a calibration lamp, a calibration bench and three calibration cells of various path lengths (19.8 mm, 40.2 mm and 60 mm). Both the reference calibration and the multi-points calibration were made for NO, NO_2, O_3 and SO_2. A reference calibration was taken for HCHO. The mixing ratios of certified gases were as follows: SO_2 – 679 ppmv; NO_2 – 966 ppmv; NO – 1510 ppmv; O_3 – 1000 ppmv (generated by an O_3 generator). The calibration formula was

$$C_m \times L_m = C_c \times L_c$$

C_m – measured path-integrated mixing ratio for a certain compound; L_m – length of measurement light-path; C_c – mixing ratio of standard gas; L_c – length of calibration cell.

Different equivalent mixing ratios were calculated by changing the length of calibration cells. The R^2 between calculated mixing ratios and measured mixing ratios were all approximately 1.0.

2.4. Site description

The OPSIS DOAS system was installed in the yard of the State Key Laboratory of Atmospheric Boundary Layer Physics and Atmospheric Chemistry (LAPC) (N 39° 58′, E 116° 22′), which is located between the North Third Ring Road and the North Fourth Ring Road in Beijing, China. The emitter/receiver unit of the DOAS system was installed on the roof of the east building in the yard, 8 m above the ground. The observation site of the *in situ* instruments was on the rooftop of another building 80 m away from the DOAS system (Fig. 1). Within a 2 km radius of the site, the average building height is 20 m. The average height to the south is approximately 50 m. A narrow west-to-east vegetation band is composed of lawns and deciduous trees with heights of 10–20 m. The fractional land use in

Fig. 1. Measurement site with instrument positions, three OPSIS DOAS paths in different directions and one AIOFM DOAS path. The topography is captured from Google Earth.

the area λ is as follows: buildings (λb) = 0.65, vegetation (λv) = 0.23 and roads (λr) = 0.12 (Song and Wang, 2012).

The OPSIS DOAS system was controlled by a stepping motor, which shifted the beam of the emitter/receiver unit automatically between three retro-reflectors. The absorption lengths of the three paths were 126 m, 266 m and 568 m. Path 1 (126 m) and path 2 (266 m) passed through a park area (urban background); the shortest path, path 1 in the same direction as path 2, was specifically chosen for NO measurements, which require the highest signal. The retro-reflector of path 3 (568 m) was installed on a lamp mast on the east side of the motorway so that the path was approximately 10 m above motorway level and perpendicular across the motorway (Fig. 1).

The comparison period for HCHO with the AIOFM DOAS was from Oct 1st until Oct 18th, 2009. The measurement period for all other compounds was October 2009. The AIOFM DOAS system was installed on the rooftop of a building on the east side of the motorway, 27 m above the ground. Its retro-reflector was fixed on the meteorological tower in the yard of LAPC, 16 m above the ground. Its absorption path length was 940 m. The light-path was nearly parallel to the OPSIS DOAS path 3, which was across the motorway (Fig. 1).

2.5. Data analysis

2.5.1. Data quality control

The data collected during maintenance, adjustments, and calibrations were excluded, as well as data collected during electricity failures. To ensure that adequate signal was present during the measurements, light intensity was used for data evaluation. If the data exceeded the observation range, the data were also excluded. A threshold of three times the standard deviation was used.

The integration time for the *in situ* instruments was 5 min, while a 1 min integration time was used for all compounds measured by the DOAS systems. Because there were multi-component measurements on every path, DOAS raw data have two or three data points per hour for every compound on each path. In accordance with Chinese Ambient Air Quality Standards (Ministry of Environmental Protection of the People's Republic of China, 2010), the data presented in this paper are hourly averaged data. If the data series collected during an hour was less than 75% (45 min), the hourly data were excluded. If the data collection in one day was less than 75% (18 h), that day's data series was excluded.

2.5.2. Data analysis

Statistical analysis was utilised for analysing temporal variations of compounds measured by all instruments. The maximum, minimum and mean values, as well as the diurnal variations for each compound, were calculated to provide an overview of air pollutant mixing ratios. Scatter plots and linear regressions were used for comparing the differences between the measurements from the various types of instruments.

To analyse wind influences, a new data set was constructed. The result of the OPSIS DOAS system was defined as A_i, the result of the comparison instruments as B_i, and the difference between A_i and B_i as C_i:

$$A_i = (A_1, A_2, A_3, \ldots, A_i);$$

$$B_i = (B_1, B_2, B_3, \ldots, B_i);$$

$$C_i = A_i - B_i = (A_1 - B_1, A_2 - B_2, A_3 - B_3, \ldots, A_i - B_i) = (C_1, C_2, C_3, \ldots, C_i).$$

The calculated C_i, is the subtraction of the measurements from the different instruments, which describes the differences between instruments.

The concept of the flux footprint will help to better explain the influence of the target compounds emissions (Kotthaus and Grimmond, 2012). Due to the eddy covariance on the same meteorological tower, the general footprint in unstable conditions ranged between 40 and 480 m, and between 500 and 4200 m in stable condition (Song and Wang, 2012). However, the height of the current eddy covariance measurement on the tower is 47 m above ground, while the height of the DOAS emitter/receiver was 8 m above ground. Thus the range of the footprint responded to the measurement height in this study is smaller than that described above.

2.5.3. Meteorological data

Mixing layer height (MLH), weather conditions, wind direction and wind speed were used to explore meteorological influences. A ceilometer (CL31, Vaisala, Finland) at the DOAS site was used for the determination of the MLH. MLH results were calculated by the default Vaisala algorithm written in MATLAB and based on the gradient method to analyse the backscattered laser intensity of this mini-lidar. Meteorological data records (every half hour) were obtained from the Chinese Meteorological Administration (CMA) site 54511 (N 39°48′, E 116°28′) in Beijing. According to the location of the station, the data represent the general wind conditions in the greater Beijing area. The distance between CMA site 54511 and LAPC is 21 km.

According to the weather conditions records from CMA site 54511, there were four different weather patterns during the comparison period: normal weather (sunny and cloudy periods), haze, rain and fog (the definitions of these weather patterns are defined by CMA). The following abbreviations are used: RA – rain, FG – fog, and HZ – haze.

3. Results and discussion

3.1. Temporal and spatial variations of compounds

Fig. 2 shows the linear correlations of the path-integrated vs. the *in situ* measurement for the four inorganic gases. Whereas the *in situ* analysers were located farther from the roadway, the path-integrated data from DOAS path 2 were used for this comparison because this optical path covered the background, coloured plots represent different weather conditions (Section 3.3). In general, the measurements of inorganic gases by the different measurement systems agree very well. NO, NO_2 and SO_2 mixing ratios are generally higher as measured by the DOAS than as measured by the *in situ* analysers, with regression factors of 1.13, 1.13 and 1.20, respectively. The O_3 results from the DOAS site were slightly lower than those of the *in situ* site, with a regression factor of 0.97. Small offsets between the two sites were found for NO, O_3, and SO_2, but offsets of up to 10 ppbv were found for NO_2 (further discussion in Section 3.2). Temporal variations from both sites were similar (Fig. 3), particularly with respect to NO and O_3, for which the temporal variations were nearly identical.

The NO observations from the two sites showed an accumulation during the evening hours (Fig. 3a) beginning at 16:00, and peaking at 21:00 (DOAS) and 22:00 (*in situ*). These peaks coincided with the combination of increasing road traffic, decreasing MLH and low wind speeds. The mixing ratios of the evening peak at the DOAS site and *in situ* site were 63 ppbv and 41 ppbv, respectively. By 05:00, the NO mixing ratios had decreased to approximately30 ppbv (DOAS) and 28 ppbv (*in situ*). The NO mixing ratios then increased again to morning peaks of 52 ppbv (DOAS)

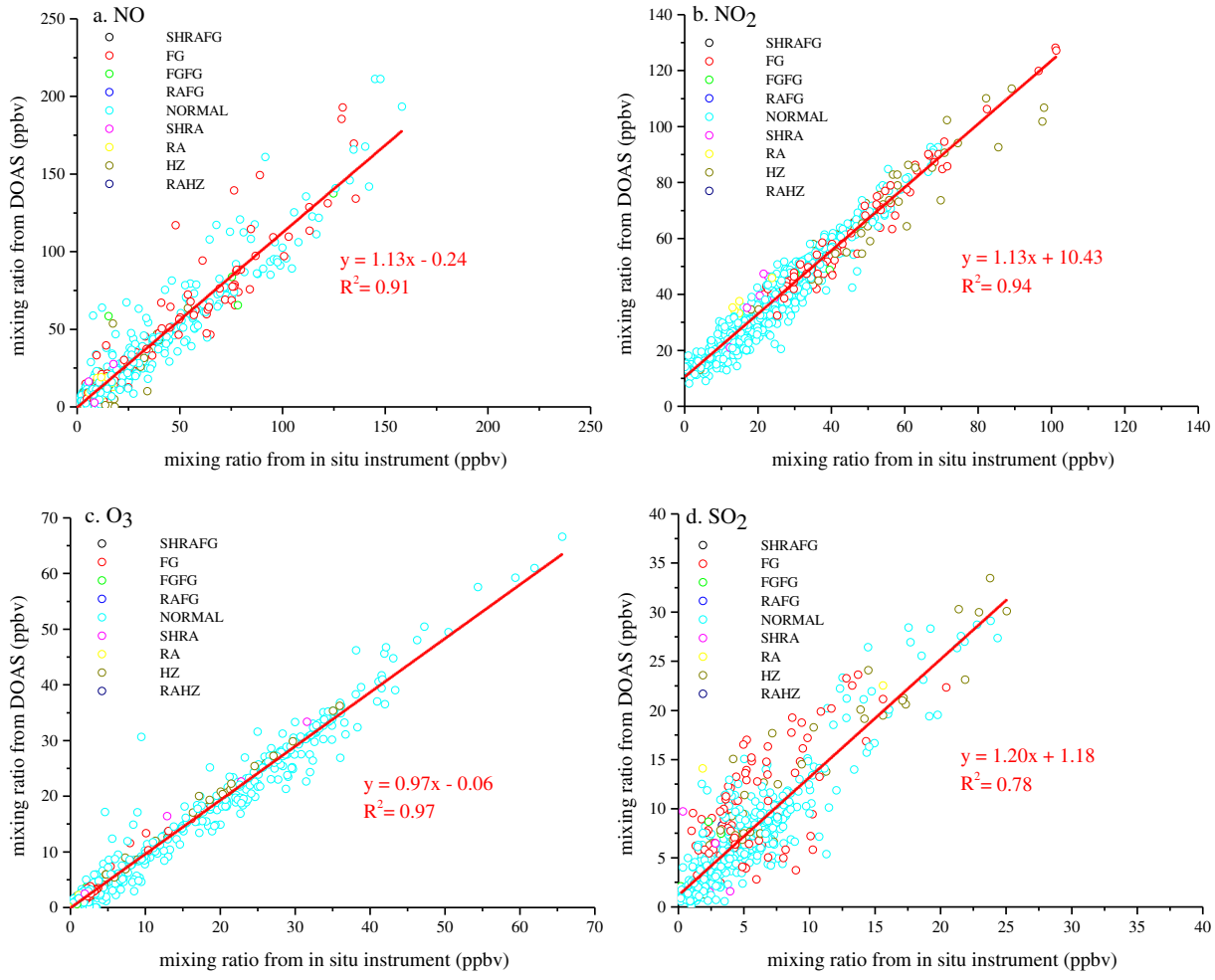

Fig. 2. Scatter plots of inorganic gases in October 2009 measured by OPSIS DOAS (path 2 – background path) and *in situ* instruments (a. NO; b. NO_2; c. O_3; d. SO_2). Coloured plots represent different weather conditions (SH – showers, RA – rain, FG – fog, BLSA – blowing sand, RA – rain, HZ – haze). (For interpretation of the references to colour in this figure legend, the reader is referred to the web version of this article.)

and 45 ppbv (*in situ*) at 07:00. Afterwards, with the increasing MLH and wind speed, NO concentrations decreased to the minimum levels of 6 ppbv at the DOAS site at 15:00 and 7 ppbv at the *in situ* site at 16:00. The higher mixing ratios as determined by DOAS, relative to the *in situ* mixing ratios, can be explained by the distance from traffic emissions. The path-integrated mixing ratio was more influenced by the streets than the *in situ* instrument, which could also explain the time delay between the peak values.

As presented in Fig. 3b, the NO_2 diurnal variation pattern had two peaks. The main peak is attributed to traffic emissions, with formation via titration between NO and O_3, decreasing MLH and wind speed. NO_2 peaked at 19:00 with mixing ratios of 61 ppbv and 42 ppbv at the DOAS site and the *in situ* site, respectively. NO_2 decreased until 05:00, reaching 38 ppbv (DOAS) and 23 ppbv (*in situ*), which were higher than the second low value that occurred during the afternoon. This gas was influenced by lower traffic emissions and the high stability of the lower atmosphere during the evening hours. The second peak, mainly caused by traffic emissions, appeared at 09:00 with values of 41 ppbv (DOAS) and 28 ppbv (*in situ*). Afterwards, mixing ratios decreased again until 13:00 to minimum values of 31 ppbv (DOAS) and 22 ppbv (*in situ*), mainly caused by an increase in the MLH and wind speed. Because a high percentage of NO_x is emitted as NO, the titration of O_3 becomes a very important source of local NO_2. Thus, direct emission and O_3 titration lead to high NO_2 peaks in the morning and evening as well as lower O_3 mixing ratios during night time. The dispersion and transport of NO_2 concentrations due to traffic emissions can affect a larger region (Suppan and Schädler, 2004).

O_3 mixing ratios showed daily variations opposite to the variations in NO (Fig. 3c). The daily peak appeared at 15:00, with mixing ratios of 29 ppbv at both the DOAS and *in situ* sites. These concentrations are due to the downward mixing air mass when the MLH increased. Meanwhile, the minimum O_3 mixing ratios appeared at 07:00, with 3 ppbv and 4 ppbv measured at the DOAS and *in situ* sites, respectively. These low O_3 mixing ratios result from NO titration during the evening as well as additional emissions of NO in the early morning.

The diurnal variation of SO_2 (Fig. 3d) had one main peak in the morning followed by several smaller peaks in the afternoon and evening. The main peak appeared at 09:00, with values of 9 ppbv from the DOAS system and 7 ppbv from the *in situ* instrument. The mixing ratios decreased until 14:00 to a low value, followed by a small peak of 8 ppbv (DOAS) and 6 ppbv (*in situ*) at 15:00. Afterwards, the trends of both instruments decreased until18:00 and then increased slowly to another peak during night time. There is no local industrial SO_2 source in Beijing, thus, SO_2 concentrations are explained by long-range transport. However, the similarity of its diurnal pattern to NO indicates there are local traffic emissions of SO_2, which can be ascribed to the sulphur content of gasoline (Fig. 3d).

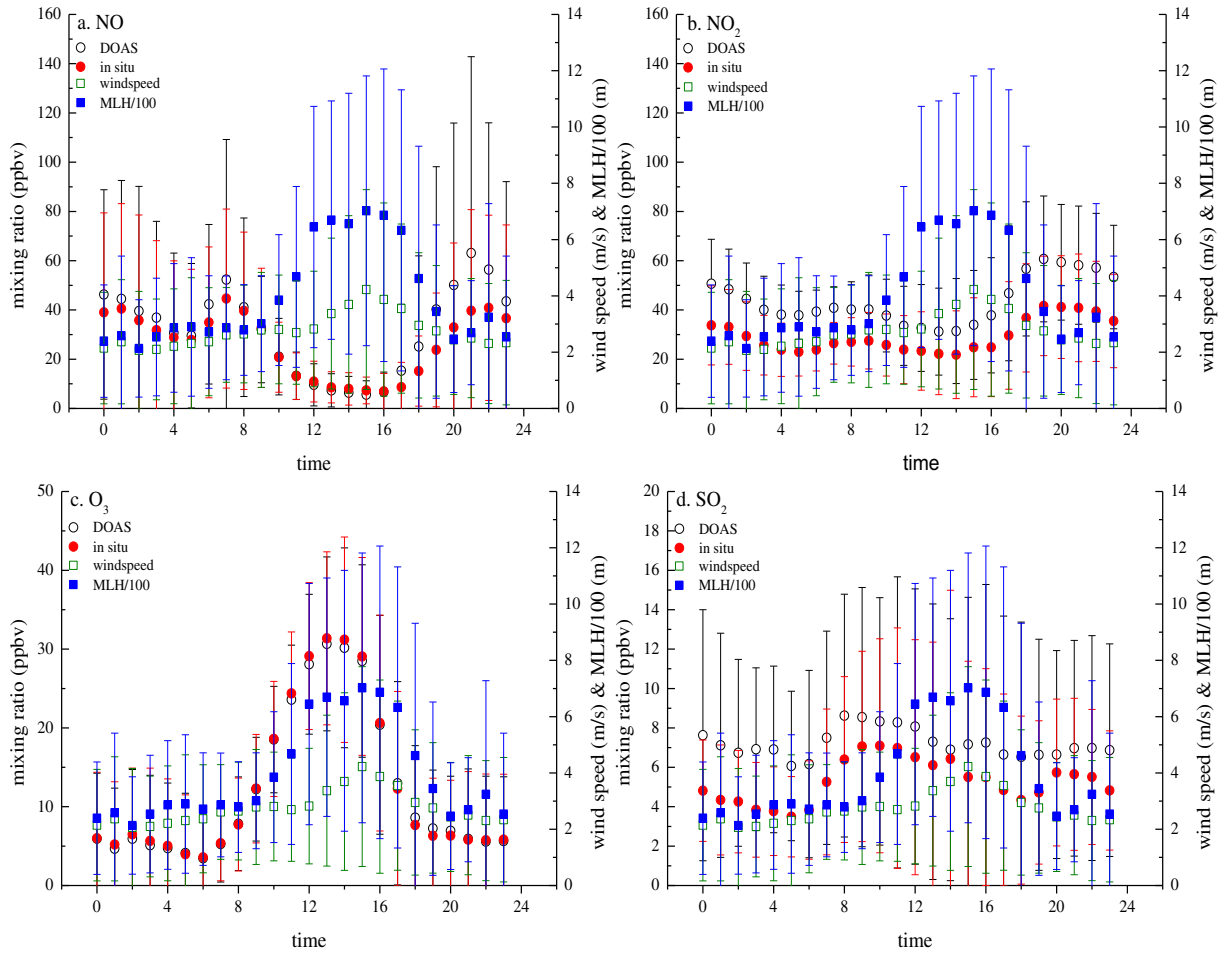

Fig. 3. Mean diurnal variations of MLH, wind speed and inorganic gas mixing ratios measured by OPSIS DOAS and *in situ* instruments (a. NO; b. NO_2; c. O_3; d. SO_2) in October 2009. Error bars denote the standard deviation for hourly intervals.

The results of the comparisons between path-integrated and *in situ* measurements show significant discrepancies for the comparisons of NO_2 and SO_2, as well as non-significant discrepancies for the comparisons of NO and O_3. The different sampling and measurement methods are the most likely causes of these discrepancies. However, they could also be related to the proximity of the traffic emissions. A steep gradient from the traffic emission source existed (further discussion in Section 3.2–3.4).

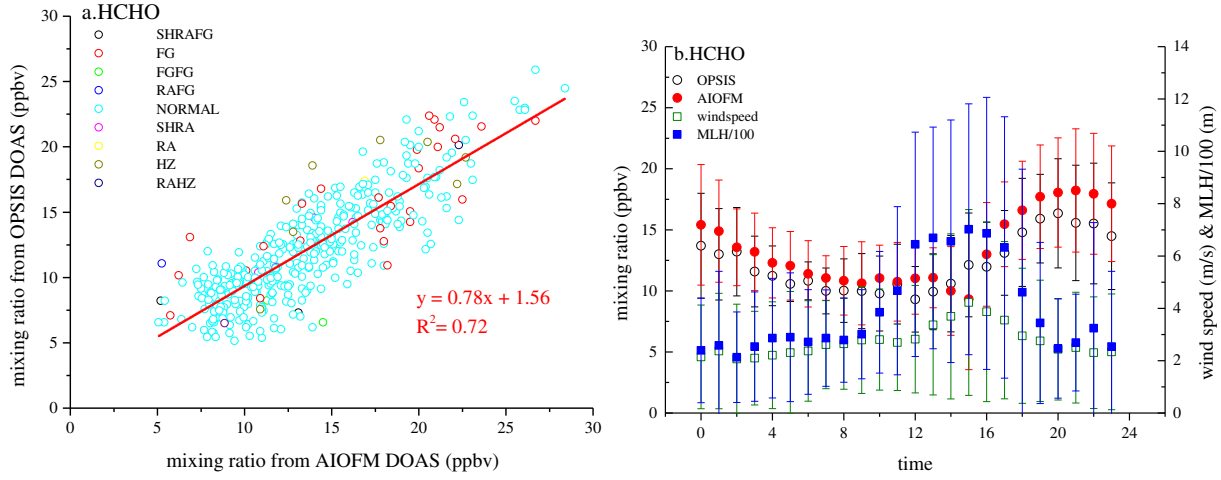

Fig. 4. Linear scatter plots of HCHO in October 2009 (a), mean diurnal variations of MLH, wind speed and HCHO mixing ratios (b), measured by OPSIS DOAS (path3 – motorway) and AIOFM DOAS. Coloured plots represent different weather conditions (SH – showers, RA – rain, FG – fog, BLSA – blowing sand, RA – rain, HZ – haze). Error bars denote the standard deviation for hourly intervals. (For interpretation of the references to colour in this figure legend, the reader is referred to the web version of this article.)

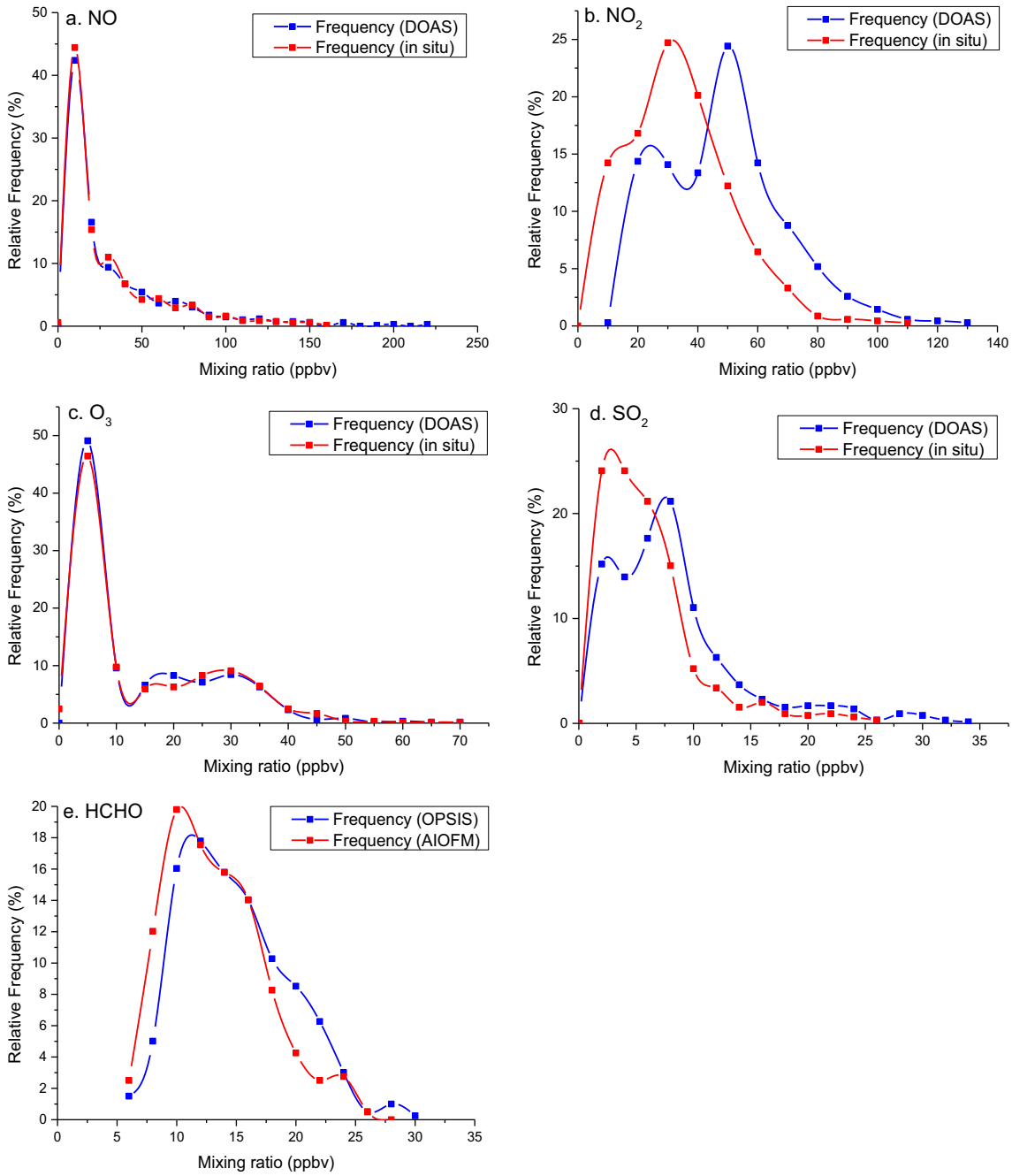

Fig. 5. The mixing ratio frequency distributions of the results of different instruments (a. NO; b. NO_2; c. O_3; d. SO_2, e. HCHO).

In conclusion, local convection and emission sources affected the temporal and spatial variations of the target compounds. Discrepancies between the measurement results of the path-integrated DOAS and *in situ* instruments were caused by the steep gradients of mixing ratios from the streets to the court yard.

The HCHO results determined by each path-integrated system were in good agreement (Fig. 4). The results from the OPSIS DOAS system were approximately 20% lower than those from the AIOFM DOAS system, with a regression factor of 0.78. The OPSIS DOAS system had an offset of approximately 1.6 ppbv in comparison to the AIOFM DOAS system. The differences between the two systems can be explained by spatial variation (further discussion in Section 3.2–3.4).

Diurnal variations of HCHO mixing ratios were observed to contain one peak (Fig. 4b, error bars denote the standard error of the mixing ratios for each hourly interval). This peak was at 19:00 with a maximum value of 18 ppbv from the AIOFM DOAS and 16 ppbv from the OPSIS DOAS system. After the peak, the mixing ratio remained at this level and gradually decreased until the morning hours.

When comparing this work to other studies in Beijing (Li et al., 2010; Pang and Mu, 2006; Pang et al., 2009), the mixing ratio range of HCHO in this campaign, between 5 and 28 ppbv, was similar to those of the other studies. However, the diurnal variations of HCHO showed different patterns. The peaks of the diurnal variations in others' work appeared at noon, while in this study, the maximum value appeared at 19:00 (Fig. 4b). The differences can be ascribed to the emission source present in the current study. There is not as much vegetation near the observation sites described here, and

therefore, the influence of biogenic VOCs is not as important. Due to the location of the motorway in the observation area, atmospheric HCHO is mainly primary HCHO from incomplete combustion; low traffic speeds and traffic jams caused high levels of HCHO emissions. The mixing ratio of HCHO began to accumulate in the afternoon. With increasing traffic flow, decreasing MLH and wind speed, the value rose gradually to the maximum value and remained high until midnight.

3.2. Mixing ratio distribution

Based on hourly mean values, the mixing ratio distributions (MRD) of five target compounds from the different measurement systems are presented in Fig. 5. Classifications from the WHO air quality guidelines and China's ambient air quality index have been used to define different regimes of mixing ratios (Table 1). There is no air quality standard for HCHO concentrations; therefore, a simple classification according the observation results has been introduced.

The MRD of NO (Fig. 5a) shows a similar distribution using the results from both DOAS and *in situ* measurements. Approximately 85% of the results were in the less polluted mode, and 10% of the results were in the slightly polluted mode. In the polluted mode (5%), the DOAS measurements show a higher proportion than the *in situ* measurements, especially the highest mixing ratio group (>160 ppbv). This group mainly resulted from the influence of the high road traffic emission, which could not be oxidised in time.

In the NO_2 MRD (Fig. 5b), most of the results were in the less polluted mode (81% of DOAS results and 89% of *in situ* results). Eighteen per cent of the DOAS measurements and 7% of the *in situ* measurements can be attributed to the slightly polluted mode and the remainder to the polluted mode. The two instruments have similar distributions, but with a shift in the maximum of the MRD by approximately 10 ppbv on average. Here too, the spatial variation of the NO_2 horizontal dispersion from the traffic emission sources led to the displacement of the distribution curves.

The O_3 MRD (Fig. 5c) of the two measurement approaches are in perfect agreement; 99% of the results were in the less polluted mode, and 1% of the results were in the slightly polluted mode.

Different spectral patterns are present in the SO_2 MRD (Fig. 5d). Forty-seven per cent of the DOAS measurements and 69% of the *in situ* measurements can be attributed to the less polluted mode, 44% and 27% of the results to the slightly polluted mode. The remaining results, 9% for DOAS and 4% for the *in situ* measurements, belong to the polluted mode. Different sampling methods resulted in the different MRD patterns and the high percentage in low mixing ratios. The differences between the methods will be especially amplified under high atmospheric humidity (discussed in Section 3.3).

Fig. 5e presents the HCHO MRD. Twenty-three per cent of the OPSIS DOAS measurements and 34% of the AIOFM DOAS measurements are in the less polluted mode, and 66% and 60% of the results are in the slightly polluted mode, respectively. The polluted mode represents 11% (DOAS) and 6% (*in situ*) of the measurements. The spectral patterns show both similarities and differences, which mainly depend on the light-paths. Although the two light-paths were nearly parallel from the top-view, the positions, path lengths and elevation angles were different. Local convection led to spatial variations in atmospheric HCHO, which resulted in the differences of the HCHO MRD of the two different DOAS systems (further discussion in Section 3.3). The HCHO MRD curve shows patterns that differ from those of the other pollutants and are similar to a Gaussian distribution. The slightly polluted mode and the polluted mode contain the majority of the measurements. This finding is additional evidence that the HCHO in the observation area was not predominantly from vegetation.

3.3. Influences of varying weather conditions on spatial variations

Weather conditions influenced the observation results of the different types of instruments deployed here. Specifically, the humidity and the MLH during different weather conditions affected the sampling methods and the diffusion of compounds. The influences of four main weather conditions (normal weather with sunny and cloudy periods, haze, rain, and fog) in the observation period are discussed individually. Table 2 summarises the regression factors and R^2 of the linear scatter plots (Figs. 2 and 4a) for target compounds between different instruments across four different weather conditions.

Decreased correlation between the DOAS and *in situ* measurements of NO was observed during the haze and the rain; these weather conditions caused most of the outliers in Fig. 2a. Less ambient O_3 led to incomplete NO titration. Thus, NO emitted from vehicles on the road could not be oxidised quickly. Low MLH, low wind speed and high humidity led to a stable atmospheric condition, which caused an NO gradient from the road to the two sites.

Although the scatter plots of NO_2 had good correlations in all types of weather conditions, the largest discrepancy, as well as the weakest linear regression between the measurements from two sites, appeared during the rain. NO_2 gradients caused by inadequate convection are an important explanation. The method used by the *in situ* instrument for NO_2 measurements is another cause. This instrument converts NO_2 into NO and then detects NO. However, a fraction of NO_y (reactive nitrogen, e.g., HNO_3, HONO, NO_3, and N_2O_5) is also converted into NO, leading to an overestimation of NO_2. In rainy periods, less NO_y is converted into NO due to the water-solubility of HNO_3 and HONO. Thus, the *in situ* results would tend to be lower than usual, resulting in a bigger discrepancy between the two sites' results.

O_3 results from both sites had reasonably good agreement across all weather conditions. The influences of weather conditions on the O_3 spatial variation in the observation area were negligible.

Decreased linear correlation of SO_2 measurements between the two sites was observed during the periods of rain and fog, which was mainly due to the sampling of the *in situ* instrument. High humidity during rain and fog influenced the measurements as water vapour may coagulate on the inner surface of the sampling

Table 1
Three pollution regimes for the five observed compounds. The same standard used for NO_2 was used for NO. The HCHO standard is a rough standard according to the observation results.

Compounds	Less polluted (ppbv)	Slightly polluted (ppbv)	Polluted (ppbv)
NO	<58 (China I)	58–97	>97 (WHO)
NO_2	<58 (China I)	58–97	>97 (WHO)
O_3	<46 (China I, WHO)	46–75	>75 (China II)
SO_2	<7 (WHO)	7–17	>17 (China I)
HCHO	<10	10–20	>20

Table 2
Regression factors and R^2 of linear scatter-plots for target compounds between different instruments under different weather conditions.

	Regression factor				R^2			
	Normal	Haze	Rain	Fog	Normal	Haze	Rain	Fog
NO	1.12	1.03	1.06	1.13	0.92	0.67	0.63	0.87
NO_2	1.16	1.02	1.01	1.17	0.93	0.90	0.81	0.96
O_3	0.97	1.02	1.02	1.06	0.97	1.00	0.99	0.94
SO_2	1.20	1.14	1.12	1.04	0.83	0.89	0.53	0.50
HCHO	0.78	0.63	0.63	0.68	0.73	0.52	0.57	0.60

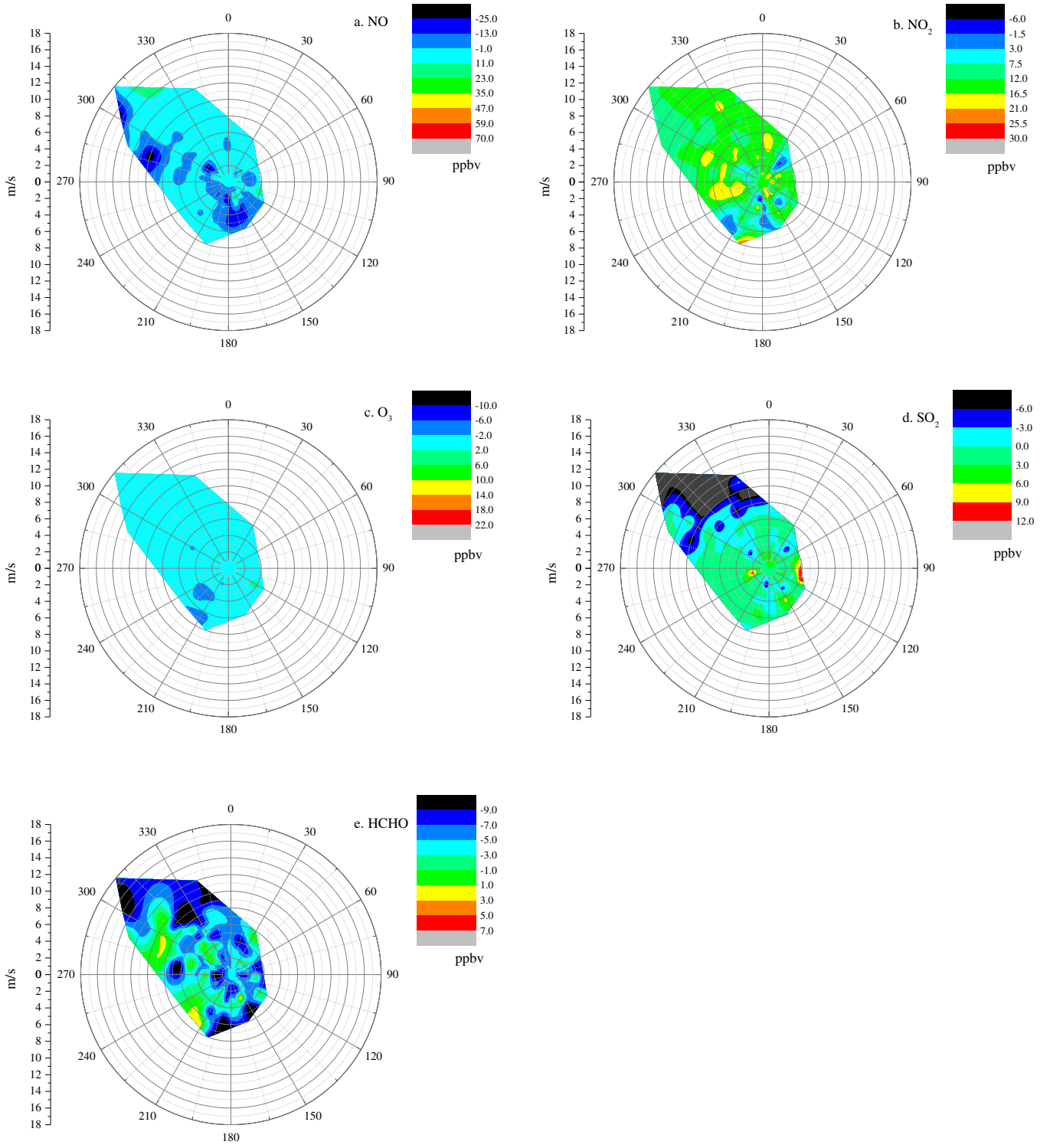

Fig. 6. Wind-rose: θ: wind direction, r: wind speed. Contours denote the discrepancies C_i between the results of the two types of instruments.

tube. When ambient air is pumped into the instrument, small quantities of SO_2 can then be absorbed by the condensate in the tube, due to its high water solubility.

For HCHO, the correlation between the results from two DOAS sites during the haze, rain and fog is worse than during normal weather conditions. The inhomogeneous spatial distributions that are attributed to different light-paths and the stable atmospheric condition are principal causes.

3.4. Influences of wind on spatial variations

Wind speed and wind direction, which are important drivers in the distribution of air pollutants, affected the comparison results in this work as well. Wind-rose figures (Fig. 6) were used to study the influences of the wind. The discrepancies, Ci, between the DOAS system and the comparison instrument (Section 2.5.2) were used for wind-rose figures. When $C_i > 0$, the OPSIS DOAS result is higher

than the comparison result; when $C_i < 0$, the OPSIS DOAS result is lower than the comparison result.

As NO was emitted from the vehicles in the streets, in principle, there should be a positive deviation when the wind was from the north. However, most of the negative deviations of NO were accompanied by northwest winds, suggesting that the local convection at the observation site was complex. There is a group of high buildings located at the south of the measurement site, which blocks the wind, resulting in surface accumulation on the north sides of the buildings when the wind arrives from the northwest. This phenomenon led to higher values from the *in situ* instruments than from the OPSIS DOAS system during northwest winds. Negative deviations were present during low wind speeds and winds from the northwest and the southeast. The low wind speed did not effectively remove the accumulated NO near the southern buildings.

The wind-rose diagram for NO_2 (Fig. 6b) also shows some areas with negative deviations, but if we consider the large differences in zero points between the two instruments (Section 3.1), all of the deviation values were positive. Those areas of yellow and orange colour had the largest positive deviations. These areas appeared mostly during periods of north and northwesterly wind direction and low wind speed, although a few occurred during periods of southerly wind direction. The north and northwesterly winds brought the NO_2 generated by traffic emissions to the observation site. An NO_2 gradient was formed from the street to the site by the north and northwesterly winds, causing positive deviations, shown in Fig. 6b. The orange area and the largest positive deviations during periods of southerly winds were mainly caused by local convection (buildings to the South).

Most of the O_3 deviation values were quite small. A few areas had negative deviations during southwesterly winds, and a few had positive deviations during periods of low wind speed from both southeasterly and northwesterly directions. Thus, ambient O_3 had no large spatial deviations. The small deviations between the OPSIS DOAS system and the *in situ* instrument were mainly caused by photochemistry and different measurement locations.

As there are no obvious SO_2 emission sources in the city of Beijing, the deviations of SO_2 results between the OPSIS DOAS system and the *in situ* instrument were influenced primarily by the wind. When the wind direction was northwesterly, the clean air mass from the mountain area removed SO_2 by dry deposition, causing the negative deviations seen in Fig. 6d. Only a few positive deviations occurred during the comparison period when the wind speed was low (for different wind directions). Positive deviations were mainly caused by local convection and the different measurement locations of the two types of instruments.

For HCHO, most of the deviations between the two different DOAS systems were negative deviations, seen in all wind directions. There was a weak relationship with wind direction but a stronger relationship with wind speed. Significant deviations always occurred in periods of high wind speed. In conclusion, different light-paths and local convection are important in explaining the differences in HCHO measurements.

4. Conclusions

As one of the most important emission sources of air pollutants in Beijing and in other cities in China, traffic emissions contribute a large portion of atmospheric pollution. Local emissions, dispersion and mixing, and long-range transport are key elements that influence urban air quality. Thus, monitoring the gaseous air pollutants emitted from motorways and busy streets is an extremely important practice. From the monitoring campaign detailed in this paper and the comparison study between the path-integrated DOAS system and *in situ* instruments, four major conclusions can be drawn:

1. The path-integrated measurements and high temporal resolution of the DOAS system best satisfy the requirements for long-term and multiple-compound monitoring of traffic-related emissions. Due to inhomogeneous emission sources and sharp gradients of air pollutants in the vicinity of streets, *in situ* instruments are less optimal.
2. Weather conditions influence the differences between the path-integrated and *in situ* measurement results, as solar radiation and the stability of the mixing layer affect local convection. Thus, removal or accumulation leads to different distributions of local air pollutants and can affect the differences between the measurement methods investigated here. In general, hazy and rainy weather lead to the weakest linear correlation between path-integrated and *in situ* measurement results.
3. Wind direction and wind speed influence the deviation between path-integrated and *in situ* mixing ratios through the transport of air pollutants. In addition, local mixing processes caused by convection processes on the micro-scale influenced by the underlying surface roughness, has an important impact on the deviations.
4. The prevailing wind system plays an important role in the removal of local air pollutants. Building positions and structures influence local convection and transport conditions.
5. Local traffic emissions led to the atypical HCHO diurnal variation in the campaign.

Acknowledgements

This study was supported by the National Natural Science Foundation of China (41230642 & 41021004) and the “Strategic Priority Research Program” of the Chinese Academy of Sciences (XDB05020000 & XDA05100100).

The work of Hong Ling in KIT/IMK-IFU was supported by China Scholarship Council (CSC).

The authors are grateful for the selfless help provided by Engineer Guangren Liu of LAPC of IAP-CAS and Wilson Lui of OPSIS.

References

Andreae, M.O., Crutzen, P.J., 1997. Atmospheric aerosols: biogeochemical sources and role in atmospheric chemistry. Science 276, 1052–1058.
Avino, P., Manigrasso, M., 2008. Ten-year measurements of gaseous pollutants in urban air by an open-path analyser. Atmospheric Environment 42, 4138–4148.
Büns, C., Kuttler, W., 2012. Path-integrated measurements of carbon dioxide in the urban canopy layer. Atmospheric Environment 46, 237–247.
Cavalcante, R.M., Campelo, C.S., Barbosa, M.J., Silveira, E.R., Carvalho, T.V., Nascimento, R.F., 2006. Determination of carbonyl compounds in air and cancer risk assessment in an academic institute in Fortaleza, Brazil. Atmospheric Environment 40, 5701–5711.
Chan, C.K., Yao, X., 2008. Air pollution in mega cities in China. Atmospheric Environment 42, 1–42.
Ebi, K.L., McGregor, G., 2008. Climate change, tropospheric ozone and particulate matter, and health impacts. Environmental Health Perspectives 116, 1449–1455.
Grosjean, D., 1982. Formaldehyde and other carbonyls in Los Angeles ambient air. Environmental Science & Technology 16, 254–262.
Grutter, M., Flores, E., Basaldud, R., Ruiz-Suárez, L.G., 2003. Open-path FTIR Spectroscopic Studies of the Trace Gases over Mexico City. In: Atmospheric and Oceanic Optics C/C Optika Atmosfery I Okeana, vol. 16, pp. 232–236.
Hao, J., Wang, L., 2005. Improving urban air quality in China: Beijing case study. Journal of the Air & Waste Management Association 55, 1298–1305.
Kotthaus, S., Grimmond, C., 2012. Identification of micro-scale anthropogenic CO_2, heat and moisture sources – processing eddy covariance fluxes for a dense urban environment. Atmospheric Environment 57, 301–316.
Lei, W., Zavala, M., De Foy, B., Volkamer, R., Molina, M.J., Molina, L.T., 2009. Impact of primary formaldehyde on air pollution in the Mexico City Metropolitan Area. Atmospheric Chemistry and Physics, 2607–2618.

Li, Y., Shao, M., Lu, S., Chang, C.C., Dasgupta, P.K., 2010. Variations and sources of ambient formaldehyde for the 2008 Beijing Olympic games. Atmospheric Environment 44, 2632–2639.
Ministry of Environmental Protection of the People's Republic of China, 2010. Ambient Air Quality Standard of People's Republic of China (in Chinese). GB 3095-2010.
Pang, X., Mu, Y., 2006. Seasonal and diurnal variations of carbonyl compounds in Beijing ambient air. Atmospheric Environment 40, 6313–6320.
Pang, X., Mu, Y., Zhang, Y., Lee, X., Yuan, J., 2009. Contribution of isoprene to formaldehyde and ozone formation based on its oxidation products measurement in Beijing, China. Atmospheric Environment 43, 2142–2147.
Platt, U., Perner, D., 1980. Direct measurements of atmospheric CH_2O, HNO_2, O_3, NO_2, and SO_2 by differential optical absorption in the near UV. Journal of Geophysical Research 85, 7453–7458.
Platt, U., Perner, D., Pätz, H.W., 1979. Simultaneous measurement of atmospheric CH_2O, O_3, and NO_2 by differential optical absorption. Journal of Geophysical Research 84, 6329–6335.
Platt, U., Stutz, J., 2008. Differential Optical Absorption Spectroscopy. Springer, Berlin Heidelberg.
Qin, M., Xie, P.H., Liu, W.Q., Li, A., Dou, K., Fang, W., Liu, J.G., Zhang, W.J., 2006. Observation of atmospheric nitrous acid with DOAS in Beijing, China. Journal of Environmental Sciences 18, 69–75.
Qin, M., Xie, P., Su, H., Gu, J., Peng, F., Li, S., Zeng, L., Liu, J., Liu, W., Zhang, Y., 2009. An observational study of the HONO-NO_2 coupling at an urban site in Guangzhou City, South China. Atmospheric Environment 43, 5731–5742.
Ravishankara, A.R., 1997. Heterogeneous and multiphase chemistry in the troposphere. Science 276, 1058–1065.
Ronneau, C., 1987. Atmospheric chemical compounds: sources, occurrence and bioassay. Eos, Transactions American Geophysical Union 68, 1643.
Schäfer, K., Emeis, S., Hoffmann, H., Jahn, C., Müller, W., Heits, B., Haase, D., Drunkenmolle, W.D., Bächlin, W., Schlünzen, K., 2005. Field measurements within a quarter of a city including a street canyon to produce a validation data set. International Journal of Environment and Pollution 25, 201–216.
Schäfer, K., Vergeiner, J., Emeis, S., Wittig, J., Hoffmann, M., Obleitner, F., Suppan, P., 2008. Atmospheric influences and local variability of air pollution close to a motorway in an Alpine valley during winter. Meteorologische Zeitschrift 17, 297–309.
Schatzmann, M., Bächlin, W., Emeis, S., Kühlwein, J., Leitl, B., Müller, W.J., Schäfer, K., Schlünzen, H., 2006. Development and validation of tools for the implementation of European air quality policy in Germany (Project VALIUM). Atmospheric Chemistry and Physics 6, 3077–3083.
Song, T., Wang, Y., 2012. Carbon dioxide fluxes from an urban area in Beijing. Atmospheric Research 106, 139–149.
Seco, R., Penuelas, J., Filella, I., 2007. Short-chain oxygenated VOCs: emission and uptake by plants and atmospheric sources, sinks, and concentrations. Atmospheric Environment 41, 2477–2499.
Seinfeld, J.H., Pandis, S.N., 1997. Atmospheric Chemistry and Physics, from Air Pollution to Climate Change. John Wiley & Sons, Hoboken, New Jersey, pp. 204–349.
Suppan, P., Schädler, G., 2004. The impact of highway emissions on ozone and nitrogen oxide levels during specific meteorological conditions. Science of The Total Environment 334, 215–222.
Volz-Thomas, A., Geiss, H., Hofzumahaus, A., Becker, K.H., 2003. Introduction to special section: photochemistry experiment in BERLIOZ. Journal of Geophysical Research 108, 8252.
Xin, J., Wang, Y., Tang, G., Wang, L., Sun, Y., Wang, Y., Hu, B., Song, T., Ji, D., Wang, W., 2010. Variability and reduction of atmospheric pollutants in Beijing and its surrounding area during the Beijing 2008 Olympic Games. Chinese Science Bulletin 55, 1937–1944.
Zhang, Y.G., Somesfalean, G., Guo, W., Wang, H.S., Wu, S.H., Qin, Y.K., Zhang, Z.G., 2012. An optical system for measuring nitric oxide using spectral separation techniques. Applied Physics B: Lasers and Optics, 1–6.